Ocean Science

Discussions

EGU

Open Access

1   # Marine climate change over the eastern Agulhas Bank of South Africa

2

3

4   Mark R Jury

5   Geography Dept, University of Zululand, KwaDlangezwa 3886, South Africa

6   and Physics Dept., University of Puerto Rico Mayaguez, USA, 00681

7   submitted to EGU ocean Sci 4 June 2020

8

9

10

11   ## Abstract

12   The rate of change in the marine environment over the eastern Agulhas Bank, along the

13   south coast of South Africa (32-37S, 20-30E) is studied using reanalysis observations 1900-2015

14   and coupled ensemble model projections 1980-2100. Outcomes are influenced by resolution and

15   time-span: ~1 degree datasets covering the whole period capture large-scale changes, while ~0.5

16   degree datasets in the satellite era better distinguish the cross-shelf gradients. Although sea surface

17   temperatures off-shore are warming rapidly (.05°C/yr since 1980), a trend toward easterly winds

18   and a stronger Agulhas Current have intensified near-shore upwelling (-.03°C/yr). The sub-tropical

19   ridge during summer is drawn poleward by global warming and high phase southern oscillation

20   index. Cooler inshore sea temperatures suppress latent heat flux and contribute to coastal desicca-

21   tion (-.005 mm day^{-1}/yr) and vegetation warming (.1°C/yr) since 1980. Coupled ensemble projec-

22   tions from the Hadley and European models indicate that the shift toward drier weather and easterly

23   winds may be sustained through the 21st century.

24

25

28

Introduction

29

30   The eastern Agulhas Bank along the south coast of South Africa is characterized by sharp

31   gradients between inshore upwelling and an offshore current that advects warm water polewards at

32   ~1 m/s (Lutjeharms et al. 2000). Downstream widening of the shelf and cyclonic shear causes

33   uplift at the shelf edge (Schumann et al. 1982, Lutjeharms 2006, Goschen et al. 2015, Malan et al.

34   2018). Westerly and easterly wind regimes during winter to summer respectively induce alternating

35   spells of downwelling and upwelling (Schumann and Martin 1991, Schumann 1999). Numerous

36   small rivers discharge into the shelf zone (Schumann and Pearce 1997, Scharler and Baird 2005,

37   vanBladeren et al. 2007). The inshore environment and large embayments (Fig 1a) are characterized

38   by weak circulations and seasonal warming, and become stratified and productive during austral

39   summer (Roberts 2010, Pattrick et al. 2013). The Agulhas Current meanders a few times per year

40   (Goschen and Schumann 1990, Rouault and Penven 2011), while the mid-latitude jet stream

41   meanders a few times per month advecting coastal lows and continental shelf waves along the shelf

42   (Jury et al. 1990, Schumann and Brink 1990). Amidst these rapid changes are rising sea levels

43   (Mather et al. 2009; Jury 2018) and longer summers.

44   The marine climate of southern South Africa is shaped by its plateau and sub-tropical

45   latitude, producing a tendency for evaporation to exceed rainfall except during high-phase Pacific

46   El Niño Southern Oscillation (ENSO), when regional atmosphere patterns couple with sea surface

47   temperatures (SST) to enhance cyclonic storms (Philippon et al. 2012). Understanding trends in

48   climate can inform resource management decisions and aid the socio-economic uptake of adaptive

49   mitigating actions. Past research has found trends of .02°C/yr in air temperature (Kruger and

50   Shongwe 2004, Morishima and Akasaka 2010, Jury 2013), however trends in other variables tend

51   to be over-shadowed by short-term events and the sparsity of data before 1950 (Tadross et al. 2005,

52   MacKellar et al. 2014, Kruger and Nxumalo 2017).

53   The main objective of this research is to establish the rate and pattern of observed and pro-

54   jected marine climate trends along the south coast of South Africa from 1900 to 2100. Scientific

55   questions include: 1) How has the wind field responded to a poleward shift of the subtropical ridge,

56   and how does that affect the shelf temperature and currents? 2) If the coastal ocean is cooling due to

57   wind- and current-driven upwelling, in contrast with the offshore environment – what are the con-

58   sequences for the local heat and water budget? 3) How does record length and dataset resolution

59   affect the result? and what is the impact of climate variability (eg. El Niño Southern Oscillation,

60   ENSO) on trend attribution? While the spatial focus is on the south coast of South Africa using

61   monthly datasets finer than 0.5°, context is provided at the large-scale using coarser model prod-

62   ucts.

Methodology

64   Modern data assimilation systems blend in-situ and ancillary measurements by iterating be-

65   tween climatology, persistence and theory, interpolating across gaps in time and space, and limiting

66   the influence of outliers. By reducing uncertainties, scientists now have a reliable means to evaluate

67   trends in marine climate. The monthly reanalysis products employed here include: ECMWF-int

68   atmosphere (Dee et al. 2011), ECMWF-20c atmosphere (Poli et al. 2016), ECMWF-ora4 ocean

69   (Balmaseda et al. 2013), NASA MERRA-2 atmosphere (Gelaro et al. 2017), NCEP CFSr-2 (Saha et

70   al. 2010), SODA-3 ocean (Carton et al. 2018), NOAA sea surface temperature (SST; Reynolds et

71   al. 2007), NOAA net outgoing longwave radiation (OLR; Lee et al. 2007), and NESDIS vegetation

72   temperature (Tucker et al., 2005). Table 1 lists the acronyms, data source, horizontal resolution and

73   time-span. Ocean-atmosphere fields with resolution finer than 50 km are capable of representing

74   cross-shelf gradients, and these are available in the satellite era 1980-2015. SODA-3 provides sub-

75   surface ocean data on temperature, salinity, currents and vertical motion; driven by MERRA-2

76   winds, multi-satellite altimeter and thermal measurements, blended with in-situ observations over

77   the shelf. Coupled land-atmosphere-ocean evolution is described by ECMWF products underpinned

78   by data assimilation (Hamrud et al 2015). Exploratory inter-comparisons of high-resolution NOAA

79   SST and surface temperature in the satellite-era reanalyses (CFSr-2, ECMWF-int, MERRA-2) show

Ocean Science
Discussions

80   coherent values and cross-shelf gradients, indicating they capture the inshore upwelling.

81   In addition to the monthly datasets, daily ECMWF-int sea level air pressure (SLP) fields

82   were analyzed using transient empirical orthogonal functions (EOF). The leading mode was deter-

83   mined and its spatial loading pattern and time score were analyzed for trends and cycling over the

84   period 1900-2015. Ship data, from the repository for marine data collected in South African waters:

85   SADCO, were analyzed in 0.1° bins for SST and wind speed, averaged 24.5-26.5°E 1950-2015 (cf.

86   Fig A1) and compared with 0.3° reanalysis products. Monthly river discharge records were ob-

87   tained for the Gamtoos and Sundays Rivers from the SA. Department of Water Affairs hydrology

88   service: SADW, and combined to understand the coastal hydrology.

89   The central method for analyzing marine climate change is to statistically regress a trend

90   line over a long record of temporal data, using the Pearson Product Moment least squares tech-

91   nique. The resultant slope and r^2 fit of the regression line provides a statistical way of determining

92   the rate of change or trend (signal) within the inter-annual fluctuations (noise). The temporal data

93   are filtered to annual and area-averages, according to the insights required.

94   Linear trends are spatially analyzed per grid point in three domains: large-scale map 45°-

95   20°S, 10°-50°E, regional-scale map: 32-37°S, 20-30°E, and depth sections over the shelf: 37-33°S,

96   averaged 24.5-26.5°E. Local trends are calculated by regression onto time series averaged over the

97   index area (35.5-33.5°S, 24.5-26.5°E) after reduction to annual and seasonal (Dec-Feb) interval. For

98   example, a sea temperature warming of 3°C over 100 years yields a .03 C/yr slope which is mapped

99   in relation to adjacent regression-fitted slopes. If year-to-year fluctuations reduce the r^2 fit below a

100   certain statistical threshold, then it is inferred that the signal is swamped by noise. Trends for U, V,

101   W wind and current components are calculated separately and combined into 'trend' vectors that

102   represent the slope or rate of change, as maps and sections. The r^2 fit of the trend is evaluated for

103   significance at 95% confidence. For long-term records having > 100 degrees of freedom, a mean-

104   ingful outcome requires $r^2 > 4\%$ (r > |0.2|). For satellite era records having < 40 degrees of freedom,

105 thresholds are reached at $r^2 > 9\%$ ($r > |0.3|$). Trends are embedded in noisy marine environments,

106 and so depend on time-span, local climate variability (Schlegel and Smit 2016), and quality of the

107 input data (Chaudhuri et al. 2013). The CFSr-2, ECMWF-int, and MERRA-2 reanalyses exhibit

108 similar trends (Kennedy et al. 2011, Decker et al. 2012) and yield comparable turbulent fluxes

109 around South Africa.

110   The trend of SST and zonal winds are analyzed by correlating the slope against its time se-

111 ries, for each month. For zonal winds, the index area is used (35.5-33.5°S, 24.5-26.5°E), but for

112 SST the analysis distinguishes between coast (33.8-33.9°S) and shelf-edge (34.9-35.0°S) latitude

113 bands. The resultant correlation values per month are plotted over the annual cycle to detect the

114 seasonality of trends in the period 1980-2015.

115   Using 18-month filtered values, hovmoller plots were constructed across the shelf to identify

116 how intra-decadal fluctuations mingle with climate change signals. After exploratory statistical

117 tests, a modulating influence was attributed to the Pacific southern oscillation index (SOI) or east-

118 west difference in SLP. Its time score is analyzed for trend and correlated with local SST and zonal

119 winds in annual and seasonal intervals 1980-2015. Similarly, a dipole mode is extracted by EOF

120 analysis of filtered ECMWF-esm projected SLP fields in the tropical Pacific, and temporal charac-

121 teristics are studied.

122   Projections of air temperature, precipitation and zonal winds from the coupled ensemble

123 ECMWF-esm v2.3 model (Taylor et al. 2012, Doblas-Reyes et al 2018) are analyzed over 1980-

124 2100 as large-scale trend maps and index-area time series. The simulation is forced by the rcp8.5

125 greenhouse scenario (vanVuuren et al. 2011, CO_2 +5 ppm /yr), and incorporates data assimilation in

126 the first 35 years that overlap with observations. Like most long-term projections, intra-member

127 dispersion is constrained by ensemble averaging and trends therefore emerge. The coupled ensem-

128 ble Hadley-esm model (Collins et al. 2011) is analyzed for zonal currents. Prior research found that

129 this model is one of the few to realistically represent ocean 'dynamic topography' (Jury 2018) and

Ocean Science
Discussions

130   sea level pressure fields around southern Africa (Dieppois et al. 2015). Its mean annual cycle of

131   zonal currents closely follows the reference Aviso-Copernicus product (cf. Fig A2).

132   An intercomparison of the reanalysis fields and model simulations is covered in the Appen-

133   dices; the above references provide insight on global validations. Ship SST and wind speed data

134   sliced in 10 km intervals describe the cross-shelf gradient in Figure A1. The coarser products (cf.

135   Table 1) under-represent the inshore upwelling, and are thus restricted to large-scale winds and

136   rainfall. Annual cycle inter-comparisons of index-area SST and zonal wind 1980-2015 are given in

137   Figure A2, and suggest that model seasonality is ~10% greater than observed.

138   **Results**

139   **Study area and large-scale trend maps**

140   The study area is illustrated in Fig 1a, and shows steep topographic and bathymetric gradi-

141   ents, with >1000 m mountains in latitudes < 33ºS, the coast at 34ºS, shelf-edge at 35ºS and deep

142   ocean to the south. The coastline is convex and indented by two bays and associated capes; the con-

143   tinental slope steepens eastward. The vegetation trend map (Fig 1b) reflects a warming rate of

144   .1ºC/yr since 1980 that increases northwest inland in conjunction with potential evaporation losses

145   (-.005 mm day^{-1}/yr). Coastal cities of Port Elizabeth and East London have slower rates of warm-

146   ing. The coarse-scale ECMWF-20c trend maps for SST and zonal wind (Fig 1c,d) reveal a warming

147   .02ºC/yr in the Agulhas Current retroflection and reduced values in the sub-tropical zones, con-

148   sistent with Dlomo (2014), where easterly winds are accelerating 1900-2010 (U = -.01 m s^{-1}/yr).

149   Easterly winds have accelerated in the south Atlantic and south Indian anticyclones and over the

150   interior of southern Africa, but in the southern mid-latitudes a westerly trend is noted over the 20th

151   century.

152   The ECMWF-20c trend map for precipitation minus evaporation (Fig 1e) indicates a grow-

153   ing deficit in the Mozambique Channel, the source region of the Agulhas Current (Fig 1f). Weaker

Ocean Science
Discussions

EGU

154 deficits are noted over the South Atlantic, while weak surplus trends are found over the eastern

155 highlands of South Africa and in the South Indian Ocean mid-latitudes. The shelf-edge Agulhas

156 Current converges and accelerates just east of the study area, then fans out and retroflects (Lutje-

157 harms 2006).

Regional ocean trend maps and sections

159 The NOAA SST trend map shows warming > .05°C/yr along the shelf edge 1981-2016 (Fig

160 2a) similar to Rouault et al. (2010). Yet inshore there is a distinct cooling trend that is faster in Al-

161 goa Bay than elsewhere (-.03°C/yr). Trends in SODA-3 salinity are weakly positive along the coast

162 in the period 1980-2015, suggesting reduced river run-off and greater evaporation. Surface layer

163 flow is accelerating in the shelf-edge Agulhas Current, particularly downstream from the study area

164 (Fig 2c). Outside the current, a pair of gyres (36°S, 25° & 29°E) directs flow toward the coast. This

165 onshore pattern has little context and may be set aside until confirmed elsewhere.

166 SODA-3 depth section trends (Fig 2d,e,f) show that the warming trend at the shelf edge is

167 aligned with an accelerating Agulhas Current (U = -.006 m s^{-1}/yr at 35.3°S; Backeberg et al. 2012).

168 The cooling trend along the coast is confined to a shallow layer < 40 m. Trends in the meridional

169 circulation reveal upwelling at depth and offshore transport in the near-shore zone. There is a sharp

170 transition to downwelling and onshore transport seaward of 35.6°S. Taken together the trend is for

171 convergence onto the Agulhas Current and faster downstream advection at the shelf edge. Changes

172 in the Agulhas Current exhibit little vertical shear, consequently cyclonic vorticity-induced uplift is

173 uniformly available but concentrated by the shelf slope (Lutjeharms 2006).

Regional wind and pressure trends

175 Trend maps are illustrated for reanalysis winds and latent heat flux in Fig 3a,b. Winds show

176 a distinct shift toward easterly winds 1980-2015, linking the South Atlantic and South Indian anti-

177 cyclones. The wind trends follow the convex coastline and divide zones of rising and falling latent

178 heat flux, consistent with the SST trends (cf. Fig 2a). The reduced moisture flux in the terrestrial

179   environment promotes hydrological deficit.

180   Regional atmospheric circulation trends were studied via EOF analysis of Dec-Feb daily

181   SLP data. This helps place the transient weather into long-term context. Mode-1 accounts for 38%

182   of variance (Fig 3c,d). Its loading pattern shows a mid-latitude antityclone passing eastward over a

183   5-day period, followed by a trough along the west coast that subsequently spawns a coastal low.

184   The mode-1 time score shows fluctuations within an upward trend (slope = .008 hPa/yr, r^2 = 11%),

185   indicating more frequent anticyclonic ridging. The gradual poleward shift of the subtropical wind

186   belt is comprized of pulsed synoptic weather.

Shelf analysis and gradients

188   Hovmoller plots were constructed across the southern shelf (Fig 4a,b) for 18-month filtered

189   surface temperature and zonal currents. Warm spells during westerly wind-driven downwelling

190   contrast with cool spells during easterly wind-driven upwelling: a multi-year alternation modulated

191   by Pacific El Nino / La Nina (Jury 2015, 2019) and the Southern Annular Mode (Malan et al.

192   2019). Yet there is a background trend toward inshore cooling and offshore warming that intensifies

193   the coastal gradient. The hovmoller plot of SODA-3 zonal currents (Fig 4b) reveals a 'pulsed' in-

194   tensification and coastward shift, contributing to near-shore uplift > 4 m/day (34.1-34.4°S). Thus

195   current- and wind-induced upwelling become additive.

196   Index-area time series of reanalysis and projected zonal currents (Fig 4c) show an accelerat-

197   ing tendency. Past and future linear regression slopes are -.0076 m s^{-1}/yr, with trend correlations

198   rising from -.81 to -.90. Future (2nd order) trends overlie those from past reanalysis and year-to-year

199   fluctuations are consistent despite technology artifacts of satellite altimetry and ensemble averag-

200   ing. Appendix A2 compares the index-area annual cycle of model vs observation.

201   The trend of NOAA SST analyzed in coastal (33.9-33.8°S) and shelf-edge (35.0-34.9°S) lat-

202   itudes show contrasting values but little change over the annual cycle in Fig 5a. Shelf-edge waters

203   are warming steadily (r= +.5) while coastal waters are cooling (r= -.5), slightly moreso from Febru-

204   ary to May (slope -.04°C/yr). Together these indicate a tightening gradient ($\partial T/\partial y$) and a steepening

205   sea slope. The annual cycle of index-area zonal wind trends (Fig 5b), averaged over three reanal-

206   yses, reveals that easterly winds are intensifying during summer (Nov-Feb), when subtropical ridg-

207   ing is most likely.

208   Regression of SST and winds onto the southern oscillation index (Fig 5c,d) reveals trend

209   patterns similar to climate change: inshore cooling (mainly summer) and offshore warming (all-

210   year). Winds with respect to high-phase SOI are from northeasterly and considerably stronger in

211   summer, hence wind-driven coastal upwelling is favoured during La Nina. The southern oscillation

212   index has shown an upward trend during the satellite era, and its regression onto regional sea level

213   air pressure patterns (cf. Fig A3) matches the earlier mode-1 pattern of mid-latitude high / sub-

214   tropical low (cf. Fig 3c). Long-term and multi-decadal trends are acknowledged to be additive here.

215   **Hydrology trends**

216   The earlier discovery of increasing near-shore salinity was related to drying trends in the ad-

217   jacent terrestrial climate, supported by declining latent heat flux (cf. Fig 3b). In Fig 5e the regional

218   hydrology is studied using the combined Gamtoos and Sundays River discharge record. Although

219   flood / drought events and 2-5 yr cycles are evident, there is no appreciable trend. The study area

220   lies between a zone of reduced cloudiness (Benguela – Namib) to the northwest and increased

221   cloudiness to the southeast, as seen in the trend map for satellite net OLR (Fig 5f). Increasing salini-

222   ty along the south coast (cf. Fig 2b) may be ascribed to advection from the Mozambique Channel,

223   where evaporation exceeds precipitation (cf. Fig 1e). Vertical motions over the shelf could also play

224   a role (cf. Fig 2f), whereby cyclonic shear lifts salty water.

225   **Model projections under greenhouse warming**

226   Spatial maps of ECWMF-esm rcp8.5 trends for zonal wind and rainfall 1980-2100 show a

227   key feature southeast of the study area (Fig 6a,b). Easterly winds are projected to increase and

228   rainfall is expected to decrease. The warm moist air carried westward beneath a stable inversion

229   layer generates less evaporation, so rain-bearing storms are projected to diminish in strength and

230   be deflected poleward by the sub-tropical anticyclone.

231   Time series of index-area values comparing ECMWF-20c reanalysis with ECMWF-esm

232   and Hadley-esm projections are given in Fig 6c-f. Coupled ensemble values overlie the observa-

233   tion-based product indicating little bias but lower variance. Zonal winds that oscillate in a station-

234   ary manner through the 20th century tend toward easterly (-U) in conjunction with declining pre-

235   cipitation. <u>Air</u> temperatures show a gradual rise during the 20th century in both reanalysis and

236   overlapping simulation. Thereafter, the warming trend steepens due to the greenhouse scenario.

237   There appears to be little moderating influence of cooler nearshore SST, which coarse resolution

238   products under-represent (cf. Fig 1c). The SOI time series is relatively stationary, but larger am-

239   plitude swings are noted in the early 20th and late 21st century. High phase (Pacific La Nina)

240   events seem steady but El Nino events appear to deepen after 2040. In summary, past zonal winds

241   of 1 m/s (after cancellation of east-west components) are projected to reach -1 m/s by 2050. Past

242   rainfall of 1.5 mm/day declines below 1 mm/day, and air temperatures of 17°C rise above 20°C

243   by 2050. The regression r^2 fit of trends are in the range from 72-97% and suggest sustained

244   changes for temperature, however wind and rain tend to oscillate in the ECMWF-esm projection

245   until the rcp8.5 scenario prevails.

246   In addition to ENSO influence, the Southern Annular Mode (SAM) plays a role in the lati-

247   tude and intensity of basin-scale anticyclonic gyres that support the Agulhas Current (Yang et al.

248   2016; Elipot and Beal 2018). The long-term trend in the SAM is a contraction of circumpolar

249   westerlies that enables poleward expansion of the tropical Hadley circulation and belt of easterly

250   winds rounding the tip of Africa seen here (cf. Fig 6a). Yet SAM trends are flattening with recov-

251   ery of the Antarctic ozone hole (Arblaster et al. 2011), and may exert less effect in future.

252   **Discussion and summary**

253   This study addressed a range of questions around spatial patterns in trends and uncovered

254   evidence of a pulsed poleward shift of the subtropical ridge (cf. Fig 3c,d). Analysis of land-

255   atmosphere-ocean conditions revealed intensified coastal upwelling from a faster shelf-edge current

256   and increased easterly wind, with consequences for coastal dessication. Employing coupled reanal-

257   ysis and model projections to distinguish coast and offshore features, a unifying process was found:

258   summer-time wind-driven upwelling enhances geostrophic gradients and the Agulhas Current. The

259   technology is reaching consensus, yet interpretations need not favour one process over another:

260   wind vs current, fluxes vs advection, multi-decadal vs trend, local vs remote. We do not expect one-

261   dimensional answers.

262   To place these results in context, trends in coastal SST were analyzed around the world. All

263   of the upwelling zones show cooling < -.03°C/yr over the satellite era: SW Africa (Namibia) 35-

264   20S, NW Africa (Sahara) 15-30N, SW America (Peru) 5-25S, NW America (California) 30-40N,

265   NE Africa (Somalia) 10-15N, and even NE America (Carolinas) 30-40N. Only the Carolinas have a

266   warm current offshore – like the south coast of South Africa, whereby the intensification of inshore

267   gradients could produce faster shelf-edge flow. However the Gulf Stream is decelerating (Jury

268   2020), unlike the Agulhas Current. Figure 4c gave evidence of a significant increase in westward

269   currents off Cape St Francis (35.5-33.5°S, 24.5-26.5°E) using low resolution ocean reanalysis and

270   coupled model projections. Yet some studies have found that wind-driven eddies are broadening the

271   Agulhas Current and that multi-year fluctuations prevail over long-term trends (Elipot and Beal

272   2018). International monitoring efforts such as the ASCA line (Morris et al. 2017) could resolve

273   ambiguities arising from the extrapolation of short-term records.

274   Another way of placing these results in perspective is to compare trends in coastal SST with

275   variance from the annual cycle (i), inter-annual variability (ii), and intra-seasonal fluctuations (iii).

276   The index-area standard deviations are: 2.5°C (i), 0.7°C (ii), and 0.9°C (iii) respectively, compared

277   with a 35-yr decline in coastal SST of -2.4°C. Applying linear regression to coastal SST data with

278   and without the annual cycle achieves $r = -.29$ vs $-.76$. Either way the trend is significant, not only

279   statistically but in terms of environmental impact.

280   In this study, modern reanalysis datasets have been used for mapping the marine climate

281   trends over the southern shelf of South Africa. Cross-shelf gradients in sea temperatures, latent heat

282   flux, currents and upwelling are apparent in the satellite era. SST in the offshore zone are warming

283   (.05°C/yr) since 1980 and there is a trend toward easterly winds, mainly in summer (U = -.015 m s^{-1}/yr). The shelf-edge Agulhas Current is accelerating (U = -.006 m s^{-1} /yr) due to winds over the

284   ^{1}/yr). The shelf-edge Agulhas Current is accelerating (U = -.006 m s^{-1} /yr) due to winds over the

285   west Indian Ocean (Backeberg et al. 2012) that align with the local forcing seen here. The faster

286   current and 'following' wind induces coastal uplift (Leber et al. 2017) and cooling (-.03°C/yr). As

287   the sub-tropical ridge is drawn poleward, the cross-shore gradient steepens (cf. Fig A1). Cooler

288   near-shore sea temperatures contribute to atmospheric subsidence, drying trends (-.005 mm day^{-1}/yr) and vegetation warming (.1°C/yr). Similar trends in local air-sea interactions are attributed to

289   ^{1}/yr) and vegetation warming (.1°C/yr). Similar trends in local air-sea interactions are attributed to

290   more frequent wind-driven coastal upwelling in Malan et al. (2019). Coupled ensemble projections

291   from the Hadley and European models indicate that the shift toward drier weather, easterly winds,

292   coastal upwelling and a faster Agulhas Current may be sustained through the 21st century. Some of

293   the environmental changes could benefit marine productivity and create opportunities for resource

294   adaptation. Likely socio-economic consequences include an enhanced fishery that could spark in-

295   terest in aquaculture and ecotourism.

296   While the shelf may benefit, terrestrial water resources could be headed towards greater

297   stress. Although the hydrology is transitionally located between a drying west and moistening east,

298   the Sundays River sees inter-basin transfers while the Gamtoos River depends on agricultural 're-

299   cycling'. In both cases reduced runoff linked to rainfall could inhibit freshwater fluxes to the coastal

300   ocean (cf. Fig 6b).

301   Parallel work on this geographic niche (Jury 2019, Jury and Goschen 2020) is on-going and

302   further studies will: i) compare observation and reanalysis trends, ii) consider how changing satel-

303   lite technology represents shelf dynamics, iii) quantify wind- vs current-driven upwelling, and iv)

304   analyze coupled models capable of detecting sharp coastal gradients.

Ocean Science
Discussions

Open Access

EGU

Acknowledgements

SAPSE funding support from South Africa is acknowledged. Most data derive from websites of the

IRI Climate Library, KNMI Climate Explorer and Univ Hawaii APDRC.

References

Arblaster JM, Meehl G, Karoly D. 2011. Future climate change in the southern hemisphere: Competing effects of ozone and greenhouse gases, *Geophysical Research Letters* 38: L02701, doi10.1029/2010GL045384.

Backeberg B, Penven P, Rouault M. 2012. Impact of intensified Indian Ocean winds on mesoscale variability in the Agulhas system. *Nature Clim Change* 2: 608–612.

Balmaseda MA, Mogensena K, Weaver AT. 2013. Evaluation of the ECMWF ocean reanalysis system ORAS4, *Quarterly Journal of the Royal Meteorology Society* 139: 1132–1161.

Carton JA, Chepurin GA, Chen L. 2018. SODA-3: A new ocean climate reanalysis. *Journal of Climate* 31: 6967–6983.

Chaudhuri AH, Ponte RM, Forget G, Heimbach P. 2013. A comparison of atmospheric reanalysis surface products over the ocean and implications for uncertainties in air–sea boundary forcing. *Journal of Climate* 26: 153–170.

Collins WJ, 17 co-authors. 2011. Development and evaluation of an Earth-System model – HadGEM2. *Geoscience Model Development* 4: 1051–1075.

Decker M, Brunke MA, Wang Z, Sakaguchi K, Zeng X and Bosilovich MG. 2012. Evaluation of the reanalysis products from GSFC, NCEP, and ECMWF using flux tower observations. *Journal of Climate* 25: 1916–1944.

Dee DP, 35 co-authors, 2011. The ERA-interim reanalysis: configuration and performance of the data assimilation system. *Quarterly Journal of the Royal Meteorological Society* 137: 553–597.

Dieppois B, Rouault M & New M. 2015. The impact of ENSO on Southern African rainfall in CMIP5 ocean atmosphere coupled climate models. *Climate Dynamics* 45: 2425–2442.

Dlomo X. 2014. Sea surface temperature trends around Southern Africa. *MSc thesis*, Univ. Cape Town, 61 pp. < open.uct.ac.za/bitstream/handle/11427/12828/thesis_sci_2014_dlomo_x.pdf >

Ocean Science
Discussions

Open Access

EGU

332 Doblas-Reyes FJ, 17 co-authors. 2018. Using EC-Earth for climate prediction research, *ECMWF*

333 *newsletter* 154, < www.ecmwf.int/en/newsletter/154/meteorology/ >

334 Elipot S, Beal LM. 2018. Observed Agulhas Current sensitivity to interannual and long-term trend

335 atmospheric forcings. *Journal of Climate* 31: 3077–3098.

336 Gelaro R, 30 co-authors. 2017. The Modern-Era Retrospective Analysis for Research and Applica-

337 tions, version 2 (MERRA-2). *Journal of Climate* 30: 5419–5454.

338 Goschen WS, Schumann EH. 1990. Agulhas Current variability and inshore structures off the Cape

339 Province, South Africa. *Journal of Geophysical Research* 95: 667–678.

340 Goschen WS, Bornman TG, Deyzel SHP, Schumann EH. 2015. Coastal upwelling on the far east-

341 ern Agulhas Bank associated with large meanders in the Agulhas Current. *Continental Shelf Re-*

342 *search* 101: 34–46.

343 Hamrud M, Bonavita M, Isaksen L. 2015. Kalman filter and hybrid-gain ensemble data assimila-

344 tion. Part I: EnKF implementation. *Monthly Weather Review* 143: 4847–4864.

345 Jury MR, MacArthur C, Reason C. 1990. Observations of trapped waves in the atmosphere and

346 ocean along the coast of southern Africa. *South African Geographical Journal* 72: 33–46.

347 Jury MR. 2013. Climate trends in southern Africa. *South African Journal of Science* 109: 53–63.

348 Jury MR. 2015. Passive suppression of South African rainfall by the Agulhas Current, *Earth Inter-*

349 *actions* 19: 1–14.

350 Jury MR. 2018. Puerto Rico sea level trend in regional context, *Journal of Ocean and Coastal*

351 *Management* 163: 478–484.

352 Jury MR. 2019. Meteorological controls on big waves south of Africa, *Regional Studies in Marine*

353 *Science* 27: 100538.

354 Jury MR. 2019. Environmental controls on marine productivity near Cape St Francis, South Africa,

355 *EGU Ocean Science*, doi.org/10.5194/os-2019-55.

356 Jury MR. 2020. Slowing of Caribbean through-flow, *Deep Sea Research* 2: 168,

357 doi10.1016/j.dsr2.2019.104682.

358 Jury MR. and Goschen W.S. 2020. Physical ocean-atmosphere variability over the shelf of South

359 Africa from reanalysis products. *Continental Shelf Research*, (in press).

360   Kennedy AD, Dong X, Xi B, Xie S, Zhang Y, Chen J. 2011. A comparison of MERRA and NARR

361   reanalyses with the DOE ARM SGP data. *Journal of Climate* 24: 4541–4557.

362   Kruger AC, Shongwe S. 2004. Temperature trends in South Africa: 1960–2003. *International Jour-*

363   *nal of Climatology* 24: 1929–1945.

364   Kruger AC, Nxumalo MP. 2017. Historical rainfall trends in South Africa: 1921–2015, *WaterSA*

365   43: 285–297.

366   Leber GM, Beal LM and Elipot S. 2017: Wind and current forcing combine to drive strong

367   upwelling in the Agulhas Current. *Journal of Physical Oceanography*, 47, 123–134,

368   Lee H-T, Gruber A, Ellingson RG, Laszlo I. 2007. Development of the HIRS outgoing longwave

369   radiation climate dataset. *Journal of Atmospheric and Oceanic Technology* 24: 2029–2047.

370   Lutjeharms JRE. 2006. *The Agulhas Current*. Springer, Berlin: 329 pp.

371   Lutjeharms JRE, Cooper J, Roberts MJ. 2000. Upwelling at the inshore edge of the Agulhas Cur-

372   rent. *Continental Shelf Research* 20: 737–761.

373   MacKeller N, New M, Jack C. 2014. Observed and modelled trends in rainfall and temperature for

374   South Africa: 1960–2010. *South African Journal of Science* 110: 1–13.

375   Malan N, Backeberg B, Biastoch A, Durgadoo JV, Samuelsen A, Reason C, Hermes J. 2018. Agul-

376   has Current Meanders facilitate shelf - slope exchange on the Eastern Agulhas Bank. *Journal of*

377   *Geophysical Research Oceans* 123: 4762–4778.

378   Malan NC, Durgadoo JV, Biastoch A, Reason CJ, Hermes, JC. 2019. Multidecadal wind variability

379   drives temperature shifts on the Agulhas Bank. *Journal of Geophysical Research Oceans* 124:

380   3021– 3035.

381   Mather AA, Garland GG, Stretch DD. 2009. Southern African sea levels: corrections, influences

382   and trends, *African Journal of Marine Science* 31: 145–156.

383   Morishima W, Akasaka I. 2010. Seasonal trends of rainfall and surface temperature over Southern

384   Africa. *African Study Monographs* 40: 67–76.

385   Morris T, Hermes J, Beal L, du Plessis M, Rae CD, Gulekana M, Lamont T, Speich S, Roberts M,

386   Ansorge IJ. 2017. The importance of monitoring the Greater Agulhas Current and its inter-ocean

387   exchanges using large mooring arrays. *South African Journal of Science* 113: 1–7.

388   Pattrick P, Strydom NA, Goschen WS. 2013. Shallow-water, nearshore current dynamics in Algoa

Ocean Science
Discussions

389   Bay, South Africa, with notes on the implications for larval fish dispersal. *African Journal of Ma-*

390   *rine Science* 35: 269–282.

391   Philippon N, Rouault M, Richard Y, Favre A. 2012. The influence of ENSO on winter rainfall in

392   South Africa. *International Journal of Climatology* 32: 2333–2347.

393   Poli P, 14 co-authors. 2016. ERA-20C: An atmospheric reanalysis of the Twentieth Century. *Jour-*

394   *nal of Climate* 29: 4083–4097.

395   Reynolds RW, Smith TM, Liu C, Chelton DB, Casey KS, Schlax MG. 2007. Daily high-resolution

396   blended analyses for sea surface temperature. *Journal of Climate* 20: 5473–5496.

397   Roberts MJ. 2010. Coastal currents and temperatures along the eastern region of Algoa Bay, South

398   Africa, with implications for transport and shelf-bay water exchange. *African Journal of Marine*

399   *Science* 32: 145–161.

400   Rouault M, Pohl B, Penven P. 2010. Coastal oceanic climate change and variability from 1982 to

401   2009 around South Africa. *African Journal of Marine Science* 32: 237–246.

402   Rouault MJ, Penven P. 2011. New perspectives on Natal Pulses from satellite observations. *Journal*

403   *of Geophysical Research Oceans* 116: 1–14.

404   Saha S, 51 co-authors. 2010. The NCEP Coupled Forecast System reanalysis. *Bulletin of the Ameri-*

405   *can Meteorological Society* 91: 1015–1057.

406   Scharler UM, Baird D. 2005. The filtering capacity of selected Eastern Cape estuaries, South Afri-

407   ca. *WaterSA* 31: 483–490.

408   Schlegel RW, Smit AJ. 2016. Climate change in coastal waters: time series properties affecting

409   trend estimation. *Journal of Climate* 29: 9113–9124.

410   Schumann EH. 1999. Wind-driven mixed layer and coastal upwelling processes off the south coast

411   of South Africa. *Journal of Marine Research* 57: 671–691.

412   Schumann EH, Perrins L-A, Hunter IT. 1982. Upwelling along the south coast of the Cape Prov-

413   ince, South Africa. South African Journal of Science, 78: 238–242.

414   Schumann EH, Brink KH. 1990. Coastal trapped waves off the coast of South Africa: generation,

415   propagation and current structures. *Journal of Physical Oceanography* 20: 1206–1218.

416   Schumann EH, Martin JA. 1991. Climatological aspects of the coastal wind field at Cape Town,

417   Port Elizxabeth and Durban. *South African Geographical Journal* 73: 48–51.

418   Schumann EH, Pearce MW. 1997. Freshwater inflow and estuarine variability in the Gamtoos Estu-

419   ary, South Africa. *Estuaries* 20: 124–133.

420   Tadross M, Jack C, Hewitson B. 2005. On RCM-based projections of change in southern African

421   summer climate. *Geophysical Research Letters* 32: L23713, doi:10.1029/2005GL024460.

422   Taylor KE, Stouffer RJ, Meehl GA. 2012. An overview of CMIP5 and the experiment design. *Bul-

423   letin of the American Meteorological Society* 93: 485–498.

424   Tucker CJ, Pinzon JE, Brown ME, Slayback DA, Pak EW, Mahoney R, Vermote EF, el Saleous N.

425   2005. An extended AVHRR 8 km NDVI dataset compatible with MODIS and SPOT vegetation

426   data. *International Journal of Remote Sensing* 26: 4485–4498.

427   van Bladeren D, Zawada PK, Mahlangu D. 2007. Statistical based regional flood frequency estima-

428   tion study for South Africa using systematic, historical and paleo-flood data. *Water Research*

429   *Commission Report* 1260/1/70, Pretoria.

430   VanVuuren DP, 14 co-authors. 2011. The representative concentration pathways: an overview,

431   *Climatic Change* 109: 5–31.

432

Ocean Science

Discussions

Open Access

EGU

433   **Table 1** Datasets used in the analysis, web sources are listed in acknowledgement.

ACRONYM	NAME	RESOLUTION	TIME SPAN
CFSr-2	Coupled Forecast System v2 ocean and atmosphere reanalysis	0.5 deg	1980-2015
ECMWF-int	European Community Medium-range Weather Forecasts interim atmosphere reanalysis	0.5 deg	1980-2016
ECMWF-20c	European Community Medium-range Weather Forecasts 20th century atmosphere reanalysis	1.0 deg	1900-2010
ECMWF-ora4	European Community Medium-range Weather Forecasts ocean reanalysis	1.0 deg	1958-2016
ECMWF-esm	European Community Medium-range Weather Forecasts coupled ensemble 21st century projections	1.2 deg	1980-2100
Hadley-esm	Hadley Centre coupled ensemble model 21st century projections for oceanography	1.5 deg	2005-2100
MERRA-2	Modern Era Reanalysis for Research and Applications v2 (NASA)	0.5 deg	1980-2015
NOAA	National Oceanic and Atmospheric Administration surface temperature and net outgoing longwave radiation	0.25-1.0 deg	1980-2016
SADCO SADW	S. Africa Data Centre Oceanogr. S.A. Dept. of Water Affairs	In-situ measurements	1950-2015 1980-2016
SODA-3	Simple Ocean Data Assimilation Reanalysis v3	0.5 deg	1980-2015

434

435   **Figures**
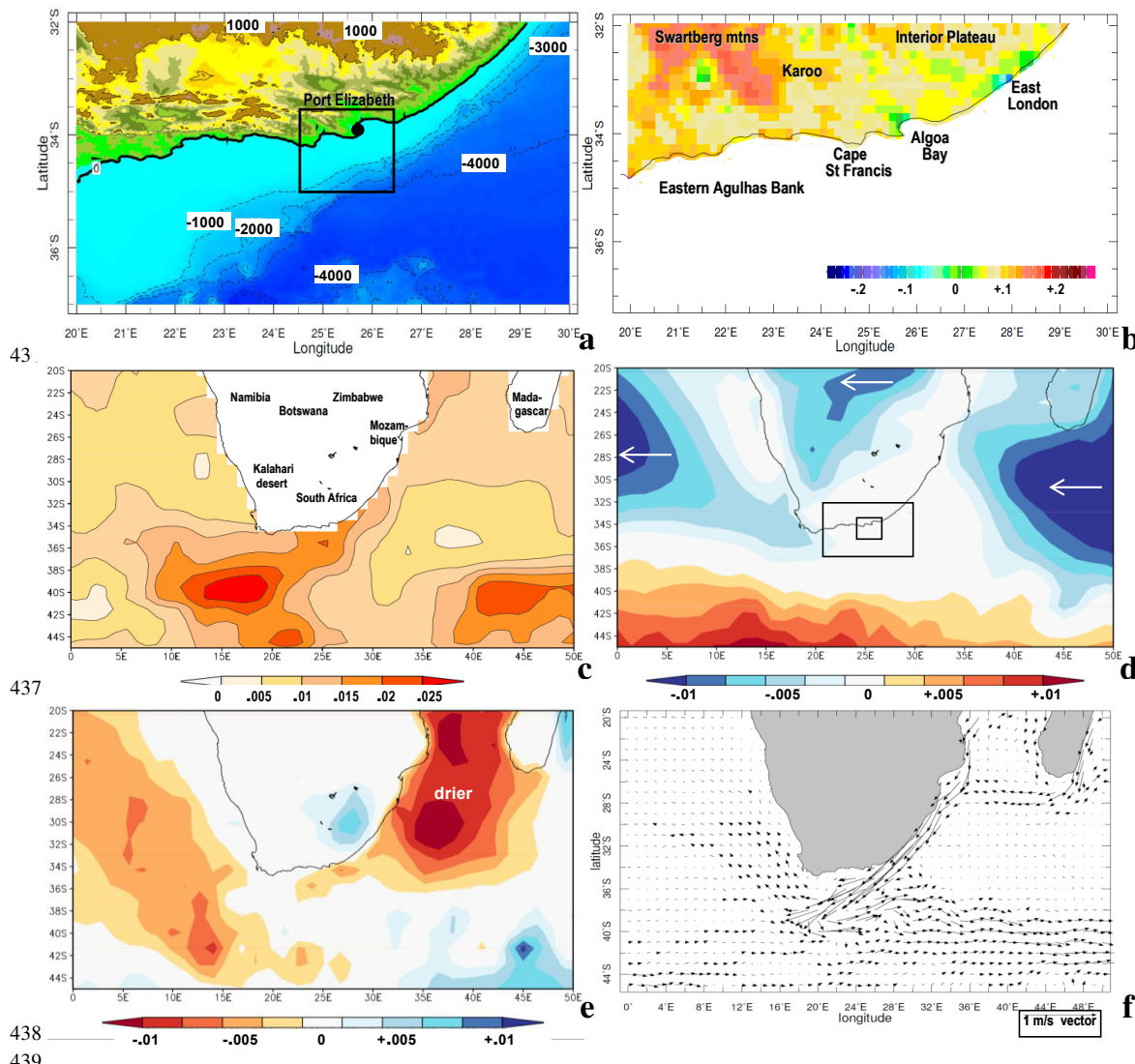
Figure 1 (a) Topography / bathymetry of the study area with index for temporal analyses (box) and Port
Elizabeth (dot). (b) Linear trend in annual NOAA vegetation temperature (C/yr 1981-2016). Large-scale
trends in annual: (c) Hadley SST (C/yr 1900-2016), (d) ECMWF-20c zonal wind (m s^{-1}/yr 1900-2010),
with inner study domains, and (e) ECMWF-20c precipitation minus evaporation trend (mm day^{-1}/yr). (f)
SODA3 mean 1-100 m currents (vector). Geographical labels are given in (b,c).

447

448

449
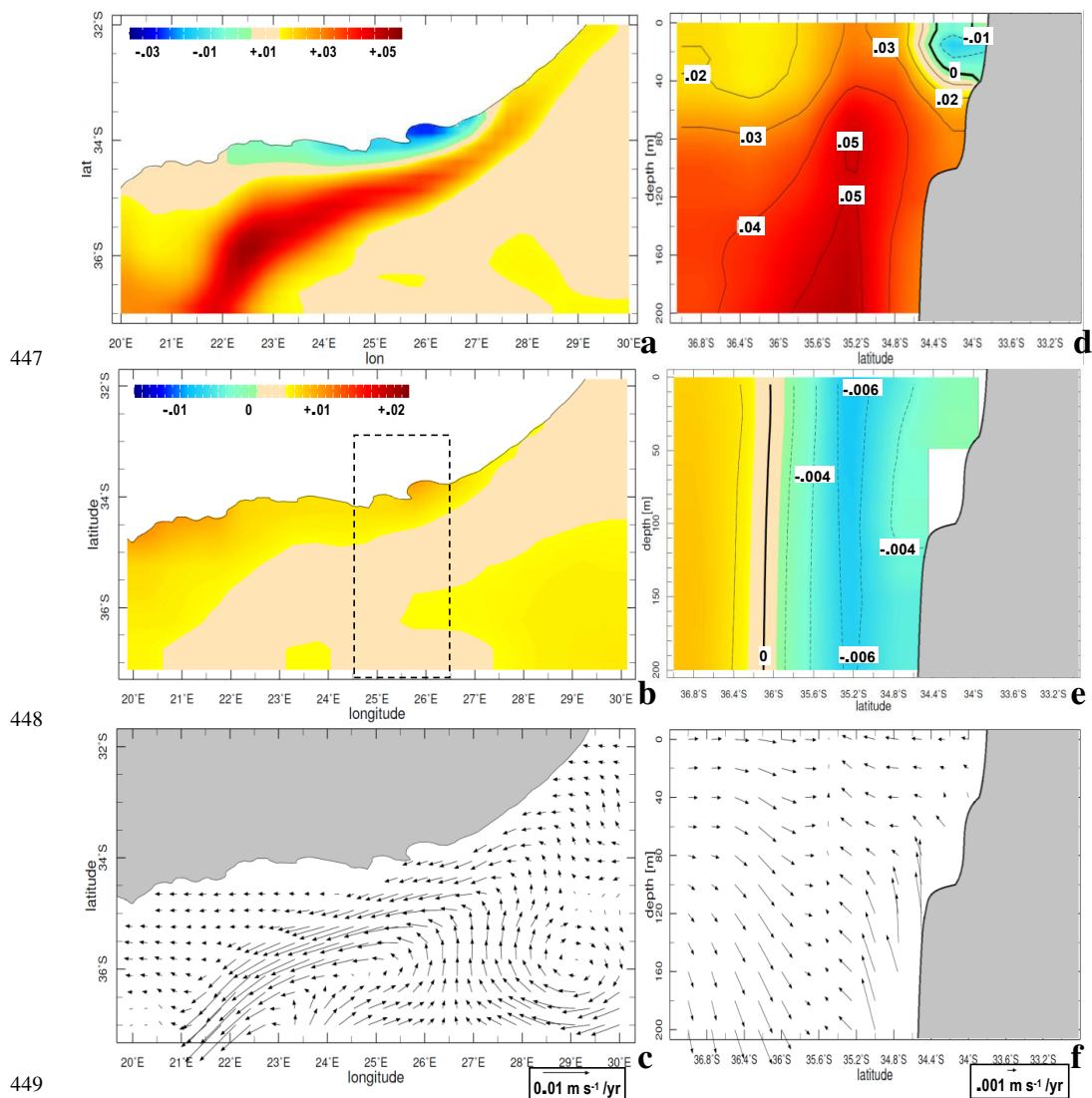
Figure 2 Regional trends in annual (a) NOAA sea surface temperature (C/yr 1981-2016); SODA-3 1980-
2015: (b) 1-10 m salinity (ppt/yr) with section denoted, and (c) 1-50 m currents (m s^{-1}/yr vector); and depth
section averaged 24.5-26.5E of (d) sea temperature (C/yr), (e) zonal current (m s^{-1}/yr), and (f) meridional
circulation (m s^{-1}/yr vector, with W exaggerated).

454

Ocean Science
Discussions

455
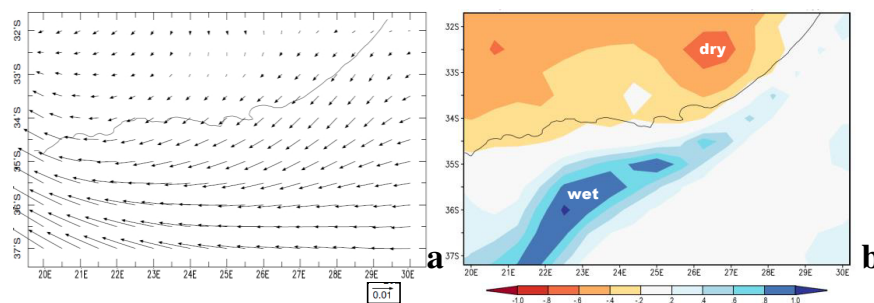
456
457

458

459
460
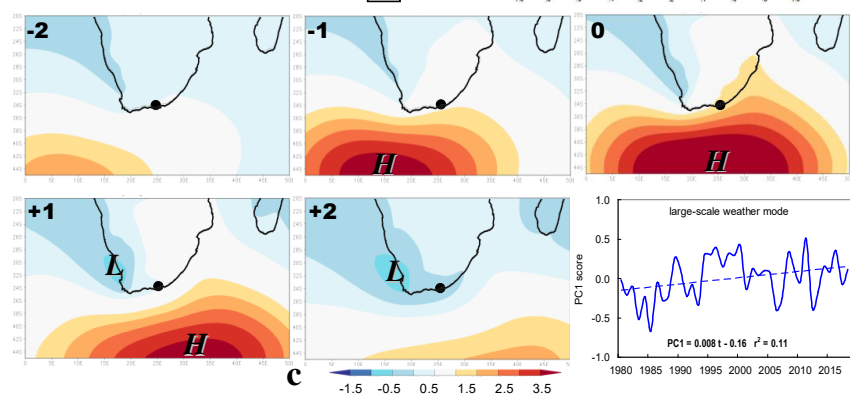
461 Figure 3 (a) Regional trend in annual CFSr-2 surface wind (m s^{-1}/yr vector, 1980-2015) and (b) latent heat

462 flux (W m^{-2}/yr). (c) Large-scale summer weather mode-1 in daily ECMWF sea level air pressure principal

463 component loading pattern at lags -2, -1, 0, +1, +2 days (hPa) and (d) time score. PC1 represents 38% of

464 variance, dot in (c) is the study area, inset in (d) is the slope and fit of the linear regression.

465

466
467
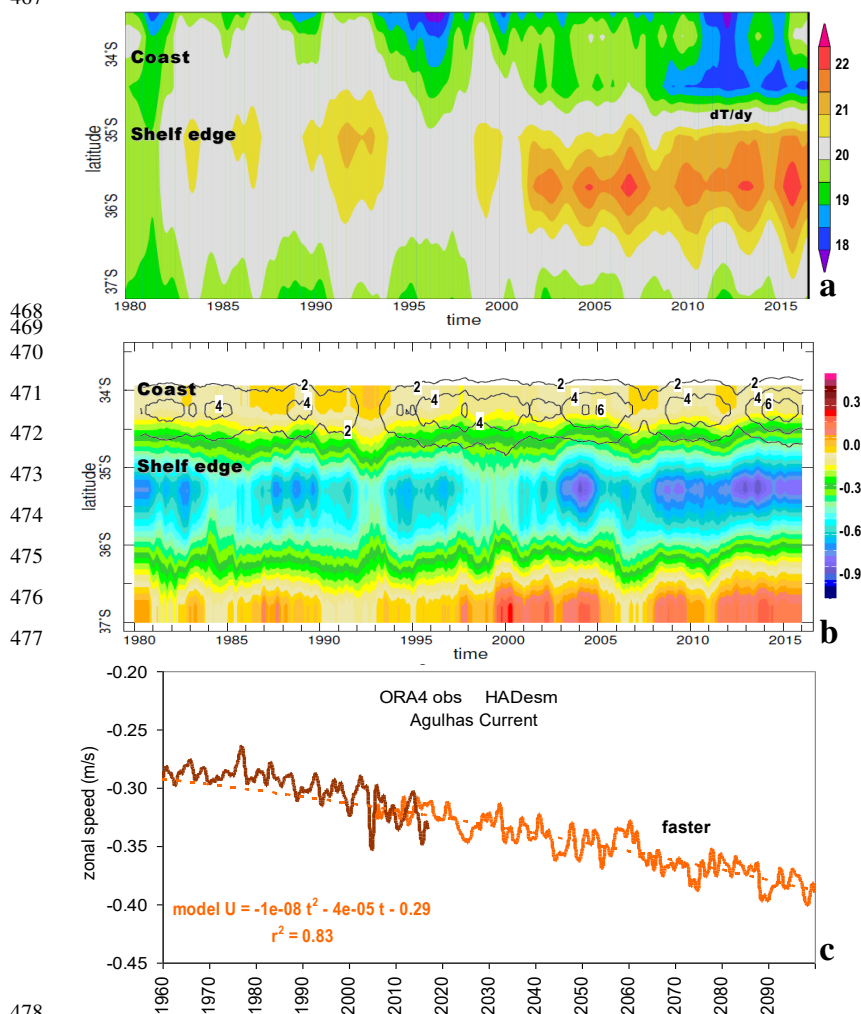
468
469
470
471
472
473
474
475
476
477

478

Figure 4 Hovmoller plots of 18-month filtered variables averaged 25-26E of ECMWF reanalysis: (a) surface temperature (C), (b) SODA-3 1-50 m zonal current (shaded m/s) and 1-200 m upward motion (contour, m/day), with coast and shelf edge denoted. (c) Index-area time series of ECMWF-ora4 observed and HAD-esm projected 1-50 m zonal current.

479
480
481
482
483

484

485

486

487
488
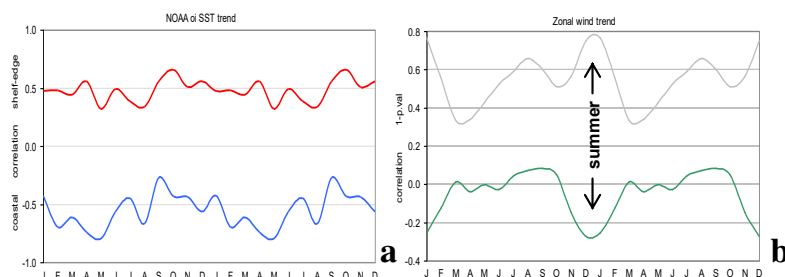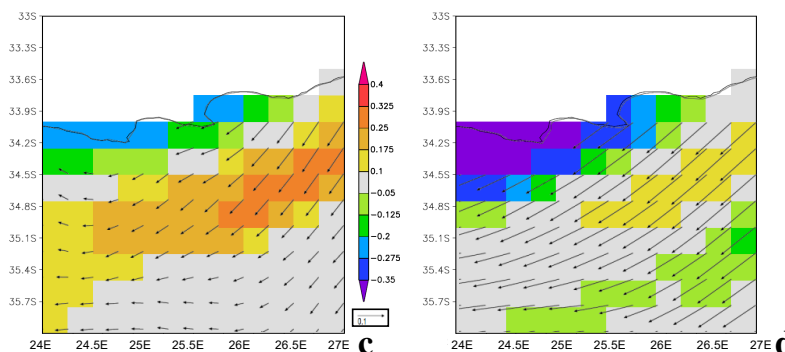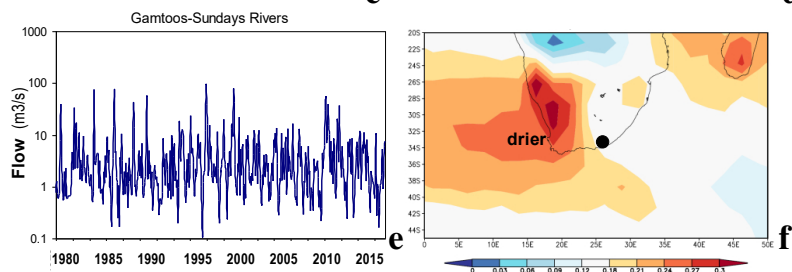
Figure 5 Analysis of monthly index-area trends for (a) coastal and shelf-edge SST, and (b) zonal wind and

its significance (1-p value), with 35 degrees of freedom. Regression of (c) annual and (d) summer NOAA

SST (shading) and SODA-3 surface wind (vector) with the SOI index 1981-2016 (units are °C and m/s per

SOI fraction). (e) Observed discharge of the combined Gamtoos and Sundays Rivers. (f) Trend of NOAA

net outgoing longwave radiation as a proxy for cloudiness (W m^{-2}/yr 1979-2017) with dot showing river

gauges.

495

496
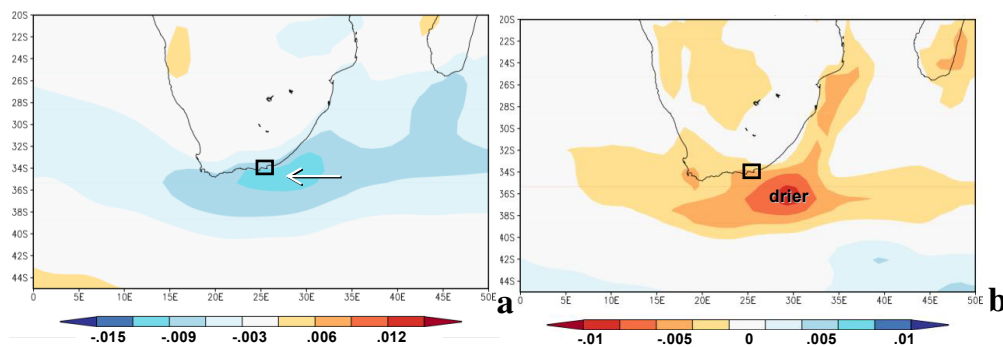
497
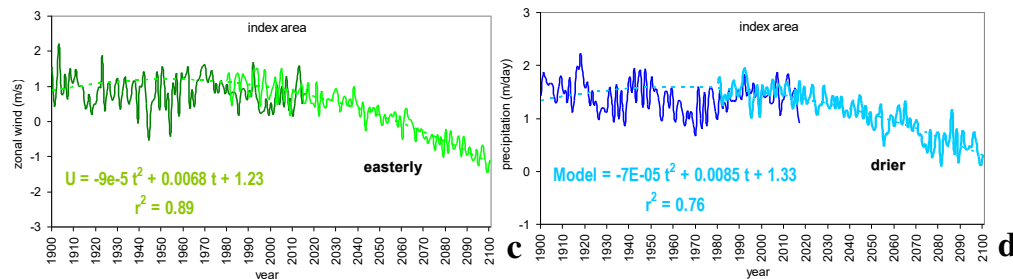
498
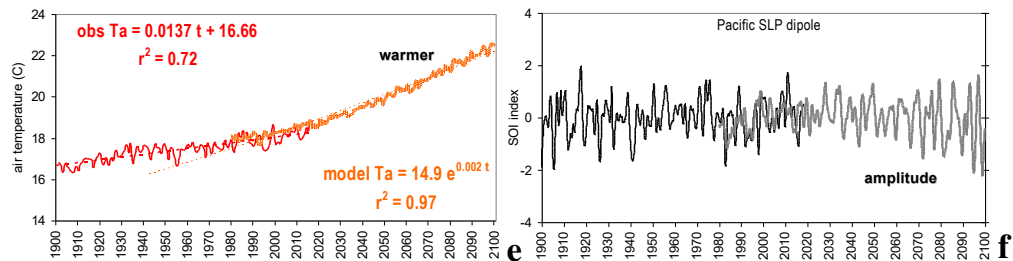
499

Figure 6 EC-esm projected trend maps 1980-2100: (a) zonal wind (m s^{-1}/yr), (b) precipitation (mm day^{-1}/yr).
Temporal record of index area ECMWF-20C reanalysis 1900-2010 and EC-esm projected 1980-2100: (c)
zonal wind, (d) precipitation, and (e) air temperature. (f) Observed and model projected Pacific southern
oscillation index (east-west SLP EOF mode). Best-fit trends are given; time series are composed of annual
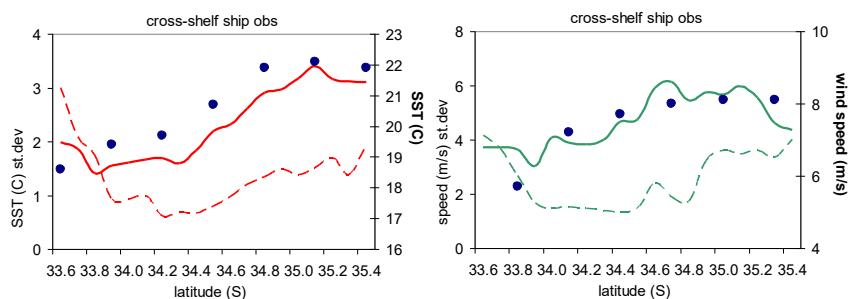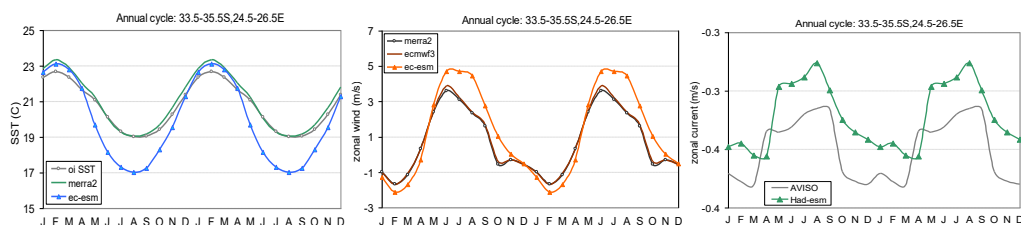averages.

505

506

Appendix

Fig A1 SADCO ship data, averages in each 0.1 latitude bin over 24.5-26.5E longitude 1950-2015; left axis and dashed line refer to standard deviation; and comparison with 0.3 binned CFSr2 (left) and ECMWF (dots).

Fig A2 Annual cycles averaged over the index area; comparing model SST, zonal wind (middle) and current with reference product. The model has an amplified annual cycle that is cooler and more westerly in winter. Currents show summer / winter regimes with model slightly weaker and delayed.
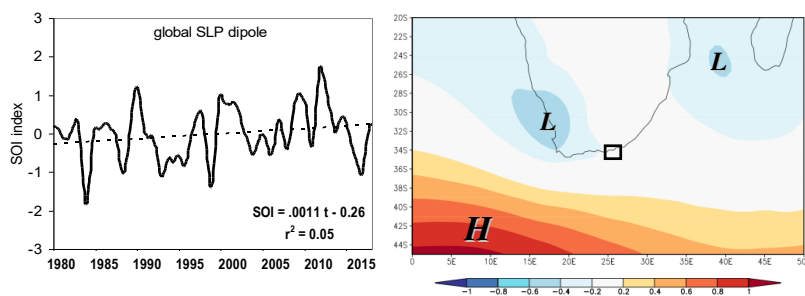
Fig A3 Graph of 18-month filtered southern oscillation index and its trend in the satellite era, and regression of Dec-Feb SOI onto regional sea level air pressure (hPa), with boxed index area.